PREPRINT - final version was published at
Sens Act. A 344 (2022), 113728, https://doi.org/10.1016/j.sna.2022.113728

Design and Modeling of An Axisymmetric Eddy Current Speed Sensor

Mehran Mirzaei*, Pavel Ripka**, Jan Machac*, Vaclav Grim***, and Jakub Svatos**
Faculty of Electrical Engineering, Czech Technical University, Prague 16627, Czech Republic

Abstract—This paper presents the design and modeling of an eddy current speed sensor for nonmagnetic moving rods with an axisymmetric configuration. The sensor consists of two antiserially connected excitation coils and one pick up coil located between two excitation coils. A novel approach using the combined finite difference method and Fourier series is proposed for the modeling and simulations of the eddy current speed sensor. The effects of the moving rod dimension and material on the performance of speed sensor are evaluated. The results of the modeling for the eddy current speed sensor are compared with the measurements at variable speeds and various frequencies. The comparison between modeling and experimental results shows the appropriateness of the eddy current speed sensor.

Index Terms—Magnetic instruments, eddy currents, speed sensor, nonmagnetic, measurement and modeling.

I. INTRODUCTION

The speed measurement is essential for control, safety, and maintenance in industrial applications [Addabbo 2019]. The precision and simplicity of the required speed sensor are both considered for the speed measurement. The speed sensors based on various physics of operations, for example, optical, variable reluctance, doppler radar and Hall sensor using permanent magnet excitation are usually utilized for rotational and translational motions. However, optical and doppler radar speed sensors are sensitive to dust and dirt. And variable reluctance and Hall sensors are destructive methodologies, which additional parts must be mounted on the conductive moving part.

An eddy current speed sensor is presented in this paper using the motional component of induced eddy currents [Feng 1975, Piao 2021, Mirzaei 2020a, Ripka 2001, Shercliff 1962, Yuan 2021] in the solid conductive moving parts. A computational tool is required for fast performance analysis and design optimization of the speed sensor [Milgravis 2020, Sato 2021]. Numerical methods using finite difference method (FDM) and finite element method (FEM) are common approaches for magnetic computations [Rodger 2021]. However, they are not cost effective for numerical calculations for all magnetic devices. Analytical methods are alternative, which are fast and enough precise for simple configurations at the constant speed [Ishida 2020, Mirzaei 2019]. Variable speeds can be considered with neglecting the acceleration in the analytical calculations [Mirzaei 2020b]. A combined analytical and finite difference method is proposed for the analysis of eddy current speed sensors at variable speeds and various frequencies. The proposed method helps to speed up modeling and reduce simulation time of the eddy current sensor, especially for non-sinusoidal field source and pulse current and time-variable speed.

II. MODEL

A. Structure and Operation Theory of Speed Sensor

Fig. 1 shows the 3D model of the axisymmetric speed sensor with two antiserially connected excitation coils and one pickup coil. The induced voltage in the pickup coil is zero at zero speed as the magnetic flux distribution is symmetric and net flux linkage in the pickup coil is zero as shown in Fig. 2. Moving rod speed causes asymmetric magnetic flux distribution and induces a voltage in the pick up coil.

B. Mathematical Formulations

The computation model can be reduced to a 2D axisymmetric structure according to Fig. 1. Therefore, the general differential equations in (1) is extracted in cylindrical coordinates [Feng 1975] for the air region, in the excitation coils and the moving rod region, respectively.

$$\frac{1}{r}\frac{\partial}{\partial r}\left(r\frac{\partial A_\phi}{\partial r}\right)+\frac{\partial^2 A_\phi}{\partial z^2}-\frac{A_\phi}{r^2}=0$$
$$\frac{1}{r}\frac{\partial}{\partial r}\left(r\frac{\partial A_\phi}{\partial r}\right)+\frac{\partial^2 A_\phi}{\partial z^2}-\frac{A_\phi}{r^2}=-\mu_0\cdot J_s,\ J_s=\frac{N_{ce}\cdot I}{w_{ce}\cdot h_{ce}}$$
$$\frac{1}{r}\frac{\partial}{\partial r}\left(r\frac{\partial A_\phi}{\partial r}\right)+\frac{\partial^2 A_\phi}{\partial z^2}-\frac{A_\phi}{r^2}=\mu_0\cdot\sigma_c\cdot\left(\frac{\partial A_\phi}{\partial t}+v\cdot\frac{\partial A_\phi}{\partial z}\right) \quad (1)$$

Where, A_ϕ is the azimuthal component of the magnetic vector potential. J_s is the current density in the excitation coil, σ_c is the solid moving rod conductivity. v is the moving rod speed. I, N_{ce}, w_{ce} and h_{ce} are the current amplitude, number of turns, axial height, and radial thickness of the excitation coils, respectively.

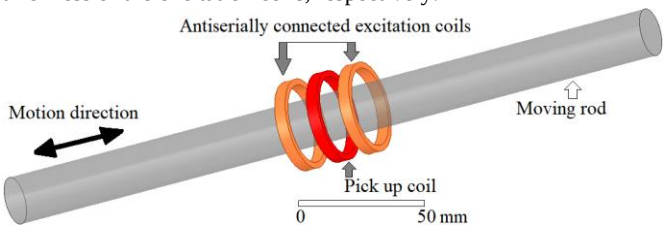

Fig. 1. 3D model of eddy current speed sensor

Corresponding author: Mehran Mirzaei (mirzameh@fel.cvut.cz).

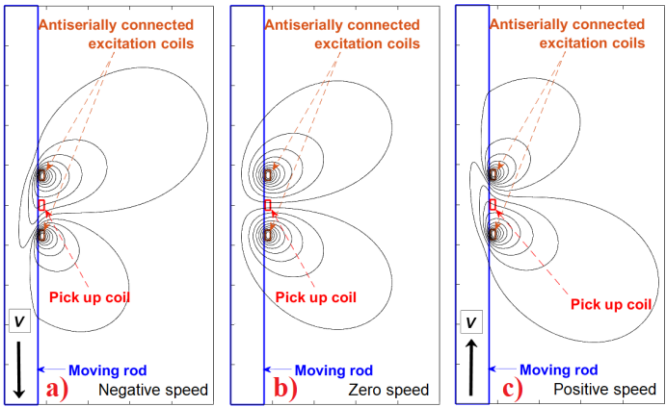

Fig. 2. Schematic magnetic flux distribution– negative speed (a), zero speed (b), and positive speed (c)

The method of separation of variables (Fourier series) is used to solve (1) in the axial *z*-direction. It is assumed that magnetic fields change periodically in the *z*-direction with period length 2*L* [Mirzaei 2019]. Parameter *L* is considered enough large to consider zero field boundary condition in outer boundary. The differentiations versus *z* could be replaced using Fourier series of sinusoidal harmonics with order *n* as follows:

$$A_\phi = \sum_m a_m \cdot e^{j(\omega t - m\cdot z)}, m = \frac{n\pi}{L}, n = \pm 1, \pm 3, \cdots$$
$$\frac{\partial A_\phi}{\partial z} = -\sum_m jm \cdot a_m \cdot e^{j(\omega t - m\cdot z)},$$
$$\frac{\partial^2 A_\phi}{\partial z^2} = -\sum_m m^2 \cdot a_m \cdot e^{j(\omega t - m\cdot z)}$$

(2)

Equations (3) and (4) are obtained by applying the finite difference method [Mirzaei 2020c] to (1) using (2) with mesh size, Δr between consecutive points (*i*-1, *i*, *i*+1) and time step, Δt between consecutive times t^k and t^{k-1}. r_i is the radius of point at position *i*. The schematic computational model is shown in Fig. 3.

$$\frac{a^k_{m,i+1} + a^k_{m,i-1} - 2a^k_{m,i}}{(\Delta r)^2} + \frac{a^k_{m,i+1} - a^k_{m,i-1}}{2r_i \cdot \Delta r} - m^2 \cdot a^k_{m,i} - \frac{a^k_{m,i}}{r_i^2} = -C \cdot \mu_0 \cdot J$$

(3)

$$J = J_{s,m} \sin(\omega t), \omega = 2\pi f$$
$$J = -\sigma_c \cdot \left(\frac{a^k_{m,i} - a^{k-1}_{m,i}}{\Delta t} - jm \cdot v(t) \cdot a^k_{m,i}\right)$$
$$\Delta t = t^k - t^{k-1}$$

(4)

Equation (4) is replaced with (5) for steady state and constant speed simulation ($\partial/\partial t = j\omega$) with excitation frequency, f ($\omega = 2\pi f$). Parameter, d in Fig. 3 is axial distance between coils.

$$J = J_{s,m}$$
$$J = -\sigma_c \cdot \left(j\omega \cdot a^k_{m,i} - jm \cdot v \cdot a^k_{m,i}\right)$$

(5)

$$J_{s,m} = \frac{2j}{n\pi}\left(\cos\left(m(d + 1.5w_{ce})\right) - \cos\left(m(d + 0.5w_{ce})\right)\right) \cdot J_s$$

(6)

Parameter, C in (3) is equal to 1 in (7) for internal parts of each region. And it is calculated according to (8), (9) and (10) at boundaries between moving rod and air region, air region and internal surface of coils and external surface of coils and air region, respectively (Fig. 3). r_r, r_{ci} and r_{co} are outer radius of moving rod, inner radius of the coils and outer radius of the coils, respectively.

$$C = 1$$

(7)

$$C = -\frac{1}{r_r} \cdot \frac{\Delta r}{4} + \frac{1}{2}$$

(8)

$$C = \frac{1}{r_{ci}} \cdot \frac{\Delta r}{4} + \frac{1}{2}$$

(9)

$$C = -\frac{1}{r_{co}} \cdot \frac{\Delta r}{4} + \frac{1}{2}$$

(10)

The induced voltage, U is calculated according to (11), (12) and (13) using magnetic vector potential, A_ϕ [Mirzaei 2019]. Ψ is the flux linkage in the pick up coil.

$$U = -\frac{d\Psi}{dt}, \quad \Psi = N_c \oint A_\phi dl$$

(11)

$$U = -\frac{\Delta\Psi}{\Delta t} = -\frac{\Psi^k - \Psi^{k-1}}{t^k - t^{k-1}}, \quad U = -j\omega \cdot \Psi$$

(12)

$$\Psi = \frac{N_{cp}\Delta r}{w_{cp} \cdot h_{cp}} \sum_{p=1,2,\ldots}^{p_c} 2\pi r_p \int_{-0.5w_c}^{0.5w_c} A_{\phi,p} dz$$
$$= \frac{N_{cp}\Delta r}{w_{cp} \cdot h_{cp}} \sum_{p=1,2,\ldots}^{p_c} 2\pi r_p \sum_m a^k_{m,p} \cdot \frac{2}{m} \cdot \sin(0.5mw_c)$$

(13)

where, N_{cp}, w_{cp} and h_{cp} are the number of turns, axial height, and radial thickness of the pick up coil, respectively. r_p is the radius of point at position, p inside pick up coil region.

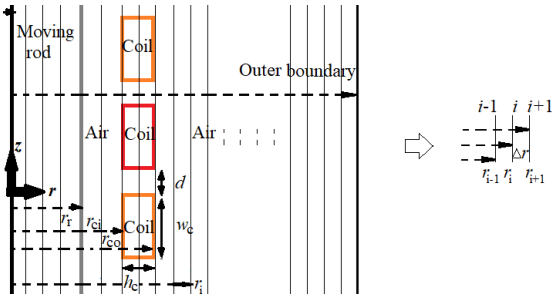

Fig. 3. Schematic model of layered mesh for eddy current sensor

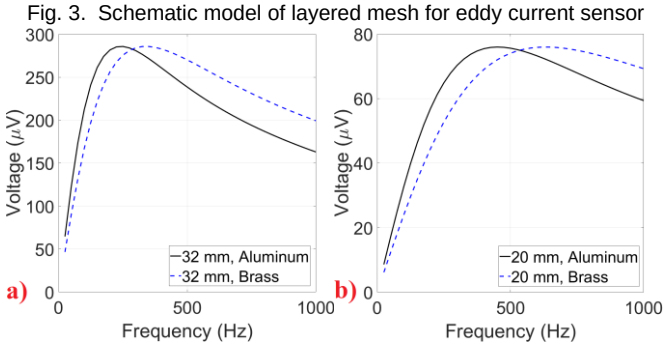

Fig. 4. The voltage amplitude of sensor versus frequency at 1 m/s – a) 32 mm rods, b) 20 mm rods (aluminum and brass)

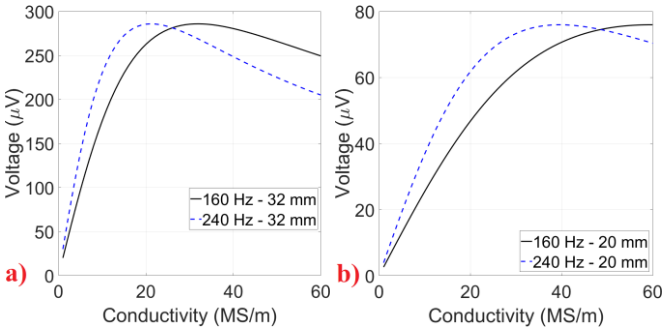

Fig. 5. The voltage amplitude of sensor versus conductivity at 1 m/s and at 160 Hz and 240 Hz– a) 32 mm rod and b) 20 mm rod

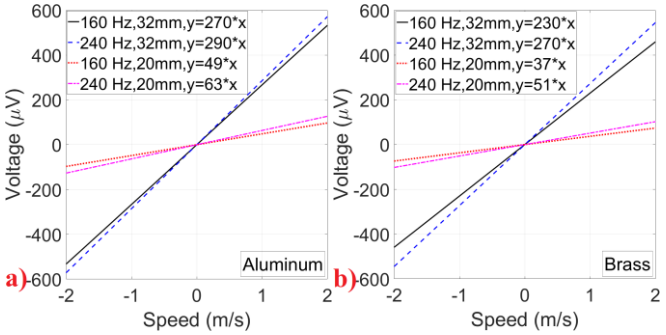

Fig. 6. - The voltage amplitude of the sensor versus speed at 160 Hz and 240 Hz– a) 32 mm and 20 mm aluminum rods and b) 32 mm and 20 mm brass rods

C. Parametric Analysis

The excitation coils and pick up coil of the sensor are identical. The coils have an inner diameter, 33 mm and an outer diameter, 38 mm with a 5 mm axial height and a 10 mm axial distance, *d* between them. Each coil has 50 turns. The moving rods have diameters, 20 mm, and 32 mm. The rod materials are brass with conductivity, 15 MS/m for both 20 mm and 32 mm rods and aluminum with different conductivities 28.5 MS/m for 20 mm rod and 21 MS/m for 32 mm rod. The frequency analysis of the eddy current sensor is presented in Fig. 4 at 1 m/s. The corresponding frequency for maximum value of the sensor voltage depends on outer diameter of the moving rod and its material conductivity. Fig. 5 shows the sensor voltage versus rod conductivity at 160 Hz and 240 Hz at 1 m/s. The maximum value of the voltage depends on the conductivity, excitation frequency and rod diameter. The sensor voltage with larger rod diameter is higher.

The amplitude of the sensor voltages versus speed displays high linearity for the aluminum and brass rods with different outer diameters, which shows the suitability of the sensor for measuring speed (Fig. 6). The sensitivities of the sensor for aluminum rods are 270 μV/m/s at 160 Hz and 290 μV/m/s at 240 Hz for 32 mm diameter and they are 49 μV/m/s at 160 Hz and 63 μV/m/s at 240 Hz for 20 mm diameter. The sensitivities are lower using brass rods as shown in Fig. 6, which are 230 μV/m/s at 160 Hz and 270 μV/m/s at 240 Hz for 32 mm diameter and 37 μV/m/s at 160 Hz and 51 μV/m/s at 240 Hz for 20 mm diameter.

III. EXPERIMENTS

The schematic view of the experimental setup is shown in Fig. 7. A digital oscilloscope, Tektronix MDO4034C with voltage resolution, 5 μV is used for the voltage measurement of the pickup coil. The excitation coil is connected to a signal generator. The speed is measured with a reference potentiometric position sensor using numerical differentiation of instantaneous relative positions of the sensor and the moving part. The instantaneous relative positions are measured by a potentiometer type position sensor. The reciprocating speed of moving rod is applied manually to avoid possible electromagnetic interference of the electric prime mover or motor on the sensor performance. The dimensions and parameters of the eddy current speed sensor for the experiments are the same as considered values in the parametric analysis.

The measured and calculated induced voltages in the pickup coil for 20 mm and 32 mm brass rods are presented in Fig. 8 - Fig. 10 and they are shown for 20 mm and 32 mm aluminum rods in Fig. 11 and Fig. 12. The speed varies in ±2 m/s range (Fig. 13). The envelopes for the induced voltage peaks of experimental and theoretical results are compared in Fig. 9 – Fig. 12.

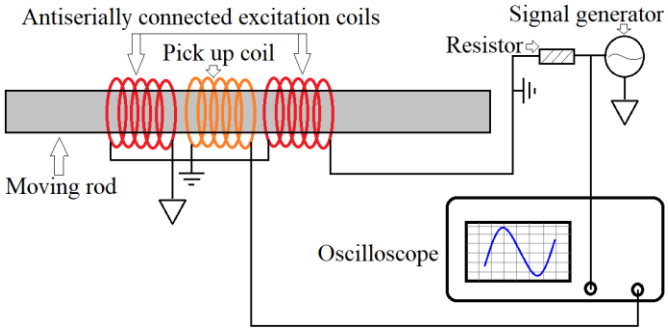

Fig. 7. Schematic view of the sensor with moving rod, signal generator and oscilloscope.

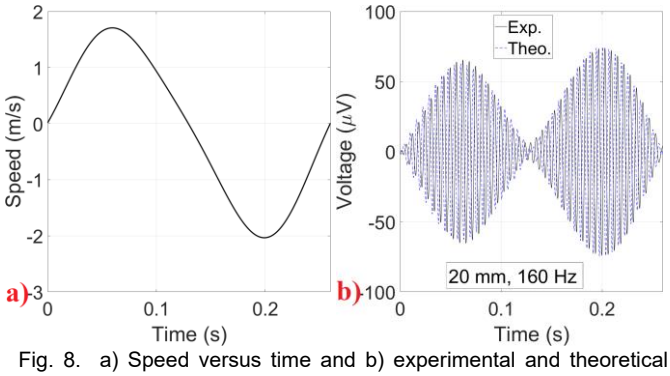

Fig. 8. a) Speed versus time and b) experimental and theoretical voltage versus time for 20 mm diameter brass rod at 160 Hz

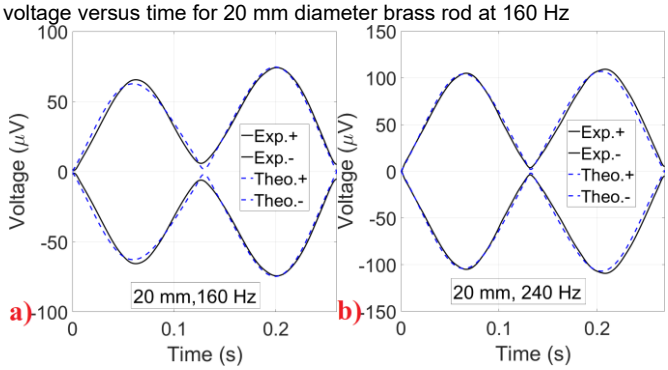

Fig. 9. Comparison between experimental and theoretical results for 20 mm diameter brass rod - a) at 160 Hz, b) at 240 Hz

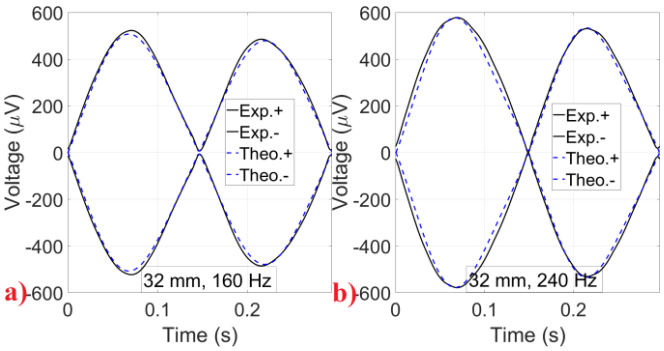

Fig. 10. Comparison between experimental and theoretical results for 32 mm diameter brass rod - a) at 160 Hz, b) at 240 Hz

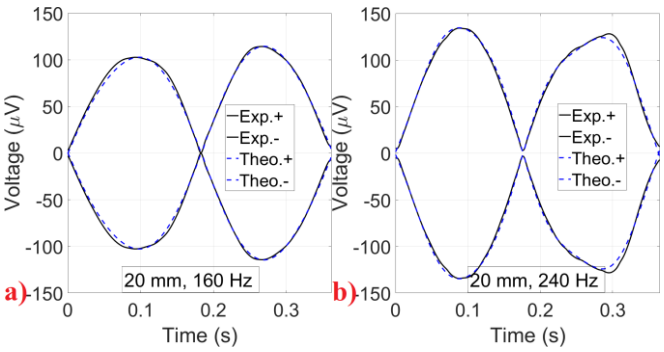

Fig. 11. Comparison between experimental and theoretical results for 20 mm diameter aluminum rod - a) at 160 Hz, b) at 240 Hz

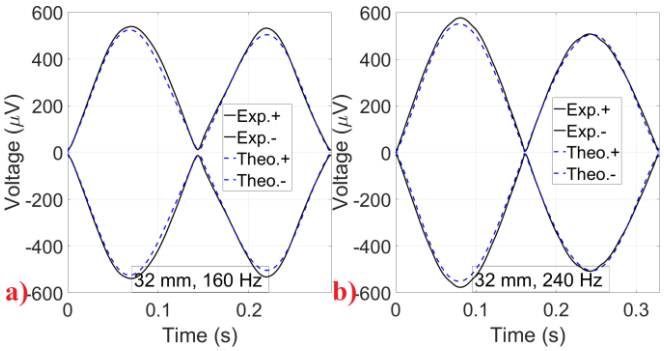

Fig. 12. Comparison between experimental and theoretical results for 32 mm diameter aluminum rod - a) at 160 Hz, b) at 240 Hz

The forms envelope of voltage peaks is like the applied speed curves to the moving rod in Fig. 13 as induced voltage is linearly proportional to the speed as presented in Fig. 6.

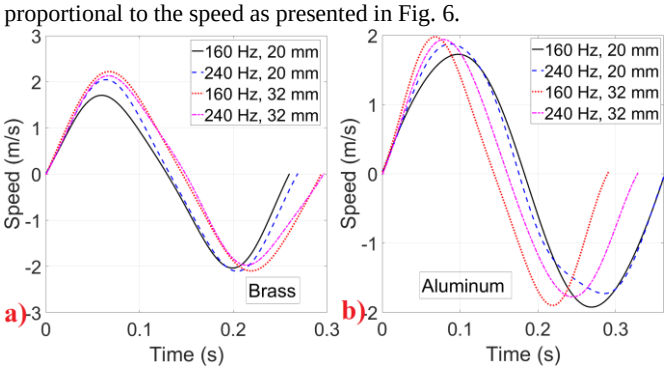

Fig. 13. Applied speeds versus time on the moving rods - a) brass rods, b) aluminum rods

The theoretical results of the induced voltage fit well with the measurements at variable speeds and excitation frequencies 160 Hz and 240 Hz as shown in Fig. 9 – Fig. 12. For example, average speed estimation error at 1 m/s is 5.5%. The main reason for the difference between measurement and theoretical results is sensor vibration effects during rod motion at variable speeds, which can be minimized by operating it at constant speed and increasing robustness of the sensor structure to avoid vibration.

IV. Discussions

The results show the high accuracy of the proposed theoretical model for the magnetic computations and performance analysis of the eddy current speed sensor at constant and variable speeds. The induced voltage of the sensor is lower at 20 mm rods; however, the measurement precision is excellent as it fits well the calculations at low voltage below 0.1 mV. The induced voltage can be converted to the speed values. As the experimental results verify that induced voltage can be used for the speed measurements as it is linearly proportional to the speed as shown in Fig. 6. The polarity of speed could be obtained by measuring the phase angle of pick up coil voltage relative to the excitation current by means of appropriate circuitry as LVDT sensors.

The movement of the rod was applied manually to avoid magnetic interference of electrical motor on the sensor performance despite its possible caused vibrations. However, the match between experimental and theoretical results may become improved with regular movement using an electrical motor as vibration effects are lower. The interference can be filtered out by postprocessing of output signal, if it is at low frequency like geomagnetic fields or higher frequencies above excitation frequencies. Lock in amplifier can be used for the precise voltage measurement when longer moving rod is used and constant speed is measured. Excitation frequencies, 160 Hz and 240 Hz were chosen, which are a compromise for the sensitivity of 20 mm and 32 mm moving rods. Using a magnetic shield or magnetic yoke around coils can also help to protect sensor against external fields and magnetic and conductive objects in the vicinity and also to increase sensitivity. The linearity range of eddy current speed sensor can be as high as ±4 m/s at excitation frequencies 160 Hz and 240 Hz. However, higher linearity range can be obtained with higher excitation frequency [Mirzaei 2020b]. Response speed of the sensor is about 4.5 ms at 160 Hz and 3.0 ms at 240 Hz.

Using the proposed theoretical method in this paper is efficient in comparison with numerical finite element method. Commercial finite element (FEM) softwares are usually used for eddy current modeling with consideration of motion. Using commercial FEM software is time consuming in terms of preprocessing, solving and postprocessing of results. Therefore, the proposed method is more covenient and cost effective. The sensitivity and voltage of the sensor decreases for 20 mm nonmagnetic rod in comparison with magnetic iron rod [Mirzaei 2019] due to the lower relative magnetic permeability, which makes it difficult to measure lower voltage. Two excitation coils and one pick up coil configuration are more suitable and reluctant to the imperfectness of the rod shape and surface and finite length of rod, because the magnetic flux distribution is more confined in the vicinity

of the coils region and the leakage flux is lower. The proposed theoretical method and sensor have no technical and theoretical limitations to be used at different speeds and accelerations. The sensitivity shownin Fig. 6 can be used to estimate different speeds of moving rod, for example, up to ±4 m/s within its high linearity range at 240 Hz and it can measure speed above 10 m/s at higher frequency, e.g., 1000 Hz. The main limitation for the sensor is the mechanical structural strength and robustness of experimental setup for the speed measurement. The proposed eddy current sensor for the measuring speed of conductive rods shows superior performances in comparison with optical and variable reluctance speed sensor in terms of simplicity, nondestructive assembly, cost-effective configuration for the sensor and signal processing unit, robustness and smaller sensitivity to dirt and dust.

V. CONCLUSION

An axisymmetric eddy current sensor for the linear speed measurement of nonmagnetic rods was presented. The theoretical approach was developed to model eddy current speed sensor at variable speed for the analysis of the sensor and parametric calculations, which is straightforward and fast. Two rods with different outer diameters are considered for the measurements and simulations. The materials of moving rods are aluminum and brass with different conductivities. The conductivities of rods were measured using 4-point measurement method. The theoretical calculations for sensor voltage match well with measurements, which approve suitability of the proposed eddy current sensor for the speed measurement of nonmagnetic moving rod with different materials and outer diameters.

The sensor requires temperature compensation as its performance is affected by the conductivity of the moving rod and its temperature dependency. Only nonmagnetic moving solid rod is considered in the paper. However, the theoretical method in this paper can be also used for the design and modeling of eddy current speed sensors with hollow rods and ferromagnetic iron moving rods.

REFERENCES

Addabbo T, Di Marco M, Fort A, Landi E, Mugnaini M, Vignoli V, and Ferretti G (2019), "Instantaneous rotation speed measurement system based on variable reluctance sensors for torsional vibration monitoring," *IEEE Trans. Inst. & Meas.*, vol. 68, pp. 2363-2373.

Feng C C, Deeds W E, and Dodd C V (1975), "Analysis of eddy-current flowmeters," *J. Applied Physics*, vol. 46, pp. 2935-2940.

Ishida K, Itaya T, Tanaka A, and Takehira N (2020), "Exact analysis of a linear velocity sensor," *IEEE Trans. Inst. & Meas.*, vol. 70, 6002106.

Milgravis M, Bojarevics A, Gaile A, and Geza V (2020), "Design of a system to compose 50 Hz alternating and static magnetic field from induction coil and permanent magnets," *IEEE Mag. Letter*, vol. 11, 2104704.

Mirzaei M, Ripka P, Chirtsov A, and Vyhnanek J (2019), "Eddy current linear speed sensor," *IEEE Trans. Mag.*, vol. 55, 4000304.

Mirzaei M, Ripka P, and Grim V (2020a), "A novel eddy current speed sensor with a Ferrite E-core," *IEEE Mag. Letter*, vol. 11, 8102905.

Mirzaei M, Ripka P, Chirtsov A, Vyhnanek J, and Grim V (2020b), "Design and modeling of a linear speed sensor with a flat type structure and air coils," *J. Magnetism and Magnetic Materials*, vol. 495, 165834.

Mirzaei M, Machac J, Ripka P, Chirtsov A, Vyhnanek J, and Grim V (2020c), "Design of a flat-type magnetic position sensor using a finite-difference method," *IET Sc., Meas. & Tech.*, vol. 14, pp. 514-524.

Piao G, Li J, Udpa L, Udpa S, and Deng Y (2021), "The effect of motion-induced eddy currents on three-axis MFL signals for high-speed rail inspection," *IEEE Trans. Mag.*, vol. 57, 6200211.

Ripka P (2001), *Magnetic Sensors and Magnetometers*, Artech House,

Rodger D (2021), "Modeling movement in electrical machines," *IEEE Trans. Mag.*, vol. 57, 8105504.

Sato M, Hattori Y, Ueda M, Bu Y, and Mizuno T (2021), "Improved performance of a flat-wire coil with magnetic composite material for wireless power transfer", *IEEE Mag. Letter*, vol. 12, 8101105.

Shercliff J A (1962), *The Theory of Electromagnetic Flow Measurement*, Cambridge University Press.

Yuan F, Yu Y, Li L, and Tian G (2021), "Investigation of DC electromagnetic-based motion induced eddy current on NDT for crack detection," *IEEE Sensors J.*, vol. 21, pp. 7449-7457.